

# JGR Biogeosciences

## RESEARCH ARTICLE

10.1029/2021JG006273

### Special Section:

The Earth in Living Color:  
Spectroscopic and Thermal  
Imaging of the Earth: NASA's  
Decadal Survey Surface

### Key Points:

- The spectrometer of NASA's Surface Biology and Geology investigation will need precise spectral calibration
- Wavelength calibration errors previously considered acceptable could result in measurement distortions far greater than the instrument noise
- Wavelength calibration inaccuracy can induce humidity-dependent biases, thwarting efforts to compare ecosystem traits across regions

### Correspondence to:

D. R. Thompson,  
[david.r.thompson@jpl.nasa.gov](mailto:david.r.thompson@jpl.nasa.gov)

### Citation:

Thompson, D. R., Brodrick, P. G., Cawse-Nicholson, K., Dana Chadwick, K., Green, R. O., Poulter, B., et al. (2021). Spectral fidelity of Earth's terrestrial and aquatic ecosystems. *Journal of Geophysical Research: Biogeosciences*, 126, e2021JG006273. <https://doi.org/10.1029/2021JG006273>

Received 4 APR 2021

Accepted 4 JUL 2021

### Author Contributions:

**Conceptualization:** David R. Thompson

**Formal analysis:** David R. Thompson

**Investigation:** Philip G. Brodrick, K. Dana Chadwick, Robert O. Green, Benjamin Poulter, Shawn Serbin











**Methodology:** David R. Thompson, Shawn Serbin, Alexey N. Shiklomanov

**Project Administration:** Benjamin Poulter

**Software:** David R. Thompson, Alexey N. Shiklomanov

© 2021. American Geophysical Union. All Rights Reserved. California Institute of Technology. Government sponsorship acknowledged. This article has been contributed to by US Government employees and their work is in the public domain in the USA.

## Spectral Fidelity of Earth's Terrestrial and Aquatic Ecosystems

David R. Thompson<sup>1</sup> , Philip G. Brodrick<sup>1</sup> , Kerry Cawse-Nicholson<sup>1</sup> , K. Dana Chadwick<sup>2</sup> , Robert O. Green<sup>1</sup> , Benjamin Poulter<sup>3</sup> , Shawn Serbin<sup>4</sup> , Alexey N. Shiklomanov<sup>3</sup> , Philip A. Townsend<sup>5</sup> , and Kevin R. Turpie<sup>6,7</sup> 

<sup>1</sup>Jet Propulsion Laboratory, California Institute of Technology, Pasadena, CA, USA, <sup>2</sup>University of Texas at Austin, Austin, TX, USA, <sup>3</sup>NASA Goddard Space Flight Center, Biospheric Sciences Lab, Greenbelt, MD, USA, <sup>4</sup>Brookhaven National Laboratories, Upton, NY, USA, <sup>5</sup>University of Wisconsin Madison, Madison, WI, USA, <sup>6</sup>University of Maryland, Baltimore County, Baltimore, MD, USA, <sup>7</sup>NASA Goddard Space Flight Center, Greenbelt, MD, USA

**Abstract** The Surface Biology and Geology (SBG) investigation will create global maps of spectral surface reflectance and emissivity at a cadence of 16 days or better, with coverage to address global questions about Earth's geology, cryosphere and ecosystems. The revolutionary potential poses a commensurate challenge: creating contiguous maps free from regional biases induced by atmosphere, observation geometry, or inversion error. This will require an accurate calibration with precise knowledge of each channel's spectral response. Here, we quantify the impact of spectral calibration on SBG's aquatic and terrestrial ecosystem objectives. We find that contemporary algorithms for ecosystem trait retrieval demand more accurate spectral calibration than historical missions. Errors due to drift or spatial nonuniformity in the wavelength calibration that have previously been considered acceptable can cause systematic errors larger than the instrument noise and of the same order as the variability SBG aims to measure. Moreover, their impact on atmospheric correction can induce climate-dependent systematic errors that thwart comparisons between ecosystems. These results underscore the importance of spectral response accuracy in SBG mission design.

**Plain Language Summary** Remote imaging spectrometers operating in visible to shortwave infrared wavelengths of the electromagnetic spectrum measure the intensity of solar-reflected light as hundreds of distinct channels. This requires knowing the precise spectral range to which each channel is sensitive. The accurate association of wavelengths to instrument channels is known as the spectral calibration of the instrument, or simply *spectral fidelity*. Small errors in this calibration can have a significant impact on measurement accuracy. This study evaluates the sensitivity of a future global investigation of Earth's ecosystems to such errors. We find that small errors in spectral calibration can cause large inaccuracies in maps of ecosystem properties. This means that accurate spectral calibration will be critical for the success of these future investigations.

## 1. Introduction

The National Aeronautics and Space Administration (NASA) commissioned a 2017 Decadal Survey report by the National Academies of Science, Engineering and Medicine to prioritize Earth science measurements in the coming decade. This report designated a global Surface Biology and Geology (SBG) investigation with Visible and Shortwave InfraRed (VSWIR) imaging spectroscopy and Thermal InfraRed (TIR) imagery (National Academies of Sciences, Engineering, and Medicine, 2018). Such instruments have a long prior history of regional airborne and orbital campaigns, but SBG's scale will be dramatically larger. It will cover Earth's entire terrestrial and coastal aquatic area at an approximate 16 day cadence. Data sharing with the European Space Agency's Copernicus Hyperspectral Imaging Mission (CHIME) (Nieke & Rast, 2018) could permit an 8–11 day cadence in some areas. It will reach regions that have been underserved by previous campaigns, such as terrestrial and aquatic biodiversity hotspots throughout South America, Sub-Saharan Africa, and Southeast Asia (Jetz et al., 2016; Myers et al., 2000; Schimel et al., 2020). SBG will provide the first global spectroscopic map and the first dense spectroscopic time series, revealing planetary processes—such as ecosystem function and biodiversity, land cover change and hydrology, and the occurrence of natural hazards—to understand the whole Earth as a system.

**Supervision:** Robert O. Green

**Writing – original draft:** David R. Thompson, Philip G. Brodrick, K. Dana Chadwick, Robert O. Green, Benjamin Poulter, Shawn Serbin, Alexey N. Shiklomanov

**Writing – review & editing:** David R. Thompson, Philip G. Brodrick, K. Dana Chadwick, Benjamin Poulter, Shawn Serbin, Alexey N. Shiklomanov

We focus here on the VSWIR component, which is likely to span the 380–2,500 nm range with approximately 10 nm spectral sampling and 30–60 m spatial resolution. It is sensitive to diverse surface properties, including: snow albedo, grain size, and contaminants; maps of sessile aquatic organisms such as seagrass and coral reefs; functional traits of terrestrial vegetation to understand ecosystem-level condition, diversity, and change; maps of mineralogy and surface composition, including soil properties and chemistry; coastal aquatic and inland water composition, productivity, and biological diversity; and more (Cawse-Nicholson et al., 2021; Schimel et al., 2020). All these VSWIR measurements involve three core operations. First, investigators calibrate sensor data to measure the spectral radiance at the sensor, that is, the intensity of reflected radiation from the surface and atmosphere in each spectral channel. Second, they invert an atmospheric Radiative Transfer Model (RTM) to estimate the hemispherical directional surface reflectance (D. R. Thompson, Babu, et al., 2019), from which view-independent reflectance quantities can be derived (Figure 1). Third, investigators analyze these reflectance and emissivity products to quantify surface properties. In all cases, the downstream analyses are only as accurate as the original radiometric measurement. Accurate spectroradiometry forms the foundation for all later analyses, and deserves special attention in mission design.

Instrument performance is often represented by *radiometry*—the accurate measurement of the radiant intensity. Radiometric performance standards are generally well understood, with studies across many disciplines (Swayze et al., 2003). Here we deal with a less common but equally important aspect of performance, the calibration of the spectral response, or simply *spectral fidelity* (Mouroulis et al., 2000). Failure to accurately calibrate the instrument spectral response can impact surface measurements by shifting or diluting reflectance features. It can also damage atmospheric correction, since imaging spectrometers estimate the atmospheric state from the data themselves, and spectral miscalibration can distort the shapes and positions of atmospheric absorptions. These errors are systematic; they do not average down over multiple observations and thus propagate directly into erroneous conclusions at the global scale. Moreover, contemporary VSWIR imaging spectrometers show more variability in spectral calibration than radiometric performance. Yet while the Decadal Survey prescribed standards for SBG radiometry, it did not give any for spectral calibration. This study fills the gap by evaluating the impact of spectral calibration on SBG objectives.

This study considers two kinds of spectral calibration errors. The first is error in the center wavelengths for each channel. This can occur due to sensor drift, but is more often caused by uncorrected spatial nonuniformities like frown (Neville et al., 2003) or twist distortions (Figure 2) that cause cross-track locations to have different wavelength centers (Richter et al., 2010). The second error involves departure of the spectral response function from the assumed—typically Gaussian—profile. This often occurs when scatter from optical surfaces broadens the spectral response, elevating the tails and blurring spectral features (D. R. Thompson, Boardman, et al., 2018; Zong et al., 2006). Figure 3 shows the effects of each distortion on the spectral response function, and Figure 4 shows the associated radiance errors. A gray overlay shows the high resolution structure of the atmospheric radiance. Wavelength shifts induce asymmetric residuals, while stray spectral response changes the apparent depth and width of atmospheric absorption features.

Several studies precede us. Nieke et al. (2008) give a comprehensive review of spectroradiometric uncertainties and their aggregate affect on radiance errors. Others assess the effect of wavelength calibration on atmospheric inversions (Dadon et al., 2010; Richter et al., 2010; Guanter, Richter, & Moreno, 2006; Kuhlmann et al., 2016; D. R. Thompson, Boardman, et al., 2018). Similar corrections appear in planetary science (Ceamanos & Douté, 2010). Green (1998) quantifies systematic errors caused by wavelength miscalibration, and in later work the impact on water vapor estimation error (Green, 2001). These prior studies generally evaluate errors in surface reflectance terms. To our knowledge no study has attempted to quantify the impact of spectral calibration on the end products of a multifaceted global investigation like SBG.

Spectral calibration accuracy is difficult to predict because it rests on a chain of optical design decisions, alignment procedures, and any software corrections (Bender et al., 2011; D. R. Thompson, Boardman, et al., 2018). Investigators have occasionally attempted post-processing to characterize and potentially correct these spectral response errors (Ceamanos & Douté, 2010; D. R. Thompson, Boardman, et al., 2018). However, there is no gold standard remedy. Corrections can introduce their own interpolation errors (Bender et al., 2011), and in any case may not fully correct the distortion (Alonso et al., 2019). Consequently, this study assesses the effects of uncorrected residual miscalibration. We first describe the experimental design,

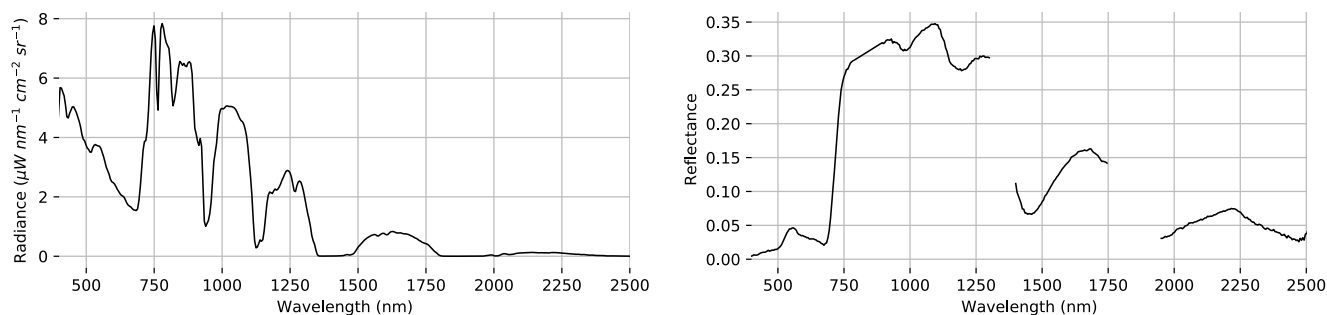


**Figure 1.** Right: Spectral radiance measured by an orbiting sensor observing vegetation. The radiance incorporates the surface reflectance but also atmospheric scattering and absorptions due to gas absorption features. Right: The associated spectral surface reflectance. Gaps in the spectrum correspond to deep water vapor absorption features that are opaque to remote sensing.

including the strategy for synthesizing, inverting, and analyzing distorted radiance spectra. We then present results and discuss implications for SBG and other future imaging spectrometer missions.

## 2. Method

We evaluate the impact of spectral calibration errors in simulation. Specifically, we define a true surface and atmospheric state and then apply an atmospheric RTM to synthesize spectral radiance at the sensor. We then simulate the measurement process, applying some level of spectroscopic distortion in either (a) wavelength center position or (b) stray spectral response. We invert the resulting distorted measurement to estimate surface reflectance, and apply downstream algorithms to evaluate the impact on the resulting products.

While SBG has many products, we focus on two benchmark cases measuring terrestrial and aquatic ecosystems. These studies are particularly challenging because they involve parts of the visible and near infrared spectrum with high contrast atmospheric and solar lines. Additionally, their global scope requires reconciling measurements acquired under a wide range of conditions. Finally, ecosystem trait and functional type analyses often rely on full-spectrum models which are finely tuned to subtle features of specific wavelengths. These factors make them likely to drive spectral calibration needs.

The first benchmark case is a vegetation functional trait analysis. These functional traits include nutrient and pigment concentrations, leaf structure, and metabolic parameters. They represent the ecological and evolutionary processes that drive plant function, and indicate plant health, efficiency, and ecosystem diversity (Cavender-Bares et al., 2020). Pigments and water content may be estimated at a leaf level by leaf RTMs (DiVittorio, 2009; Féret et al., 2017; Shiklomanov et al., 2016), but these algorithms are typically computationally intensive and require additional ancillary information such as the plant to soil ratio in the pixel. A more common alternative is to fit statistical relationships between individual spectra and chemical

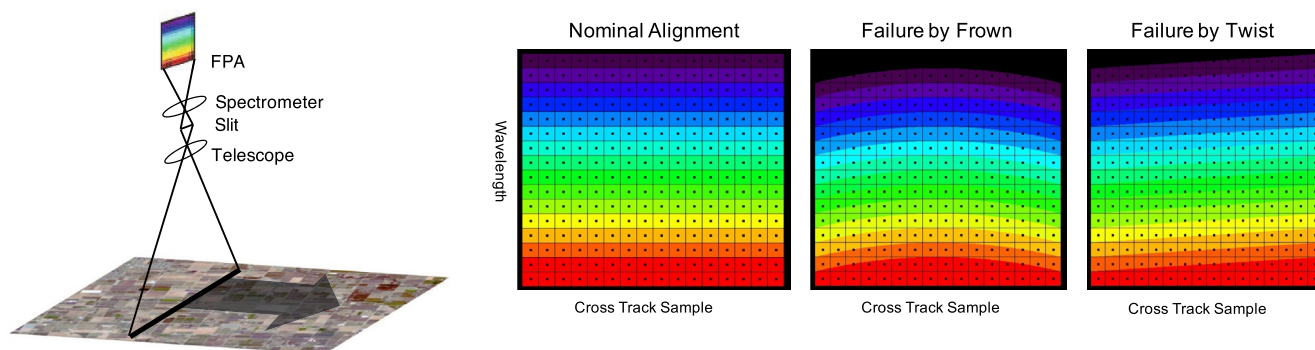


**Figure 2.** Left: The spectrometer observation system, adapted from Mouroulis et al. (2000). Center and Right: Nominal and distorted projections onto the focal plane array.

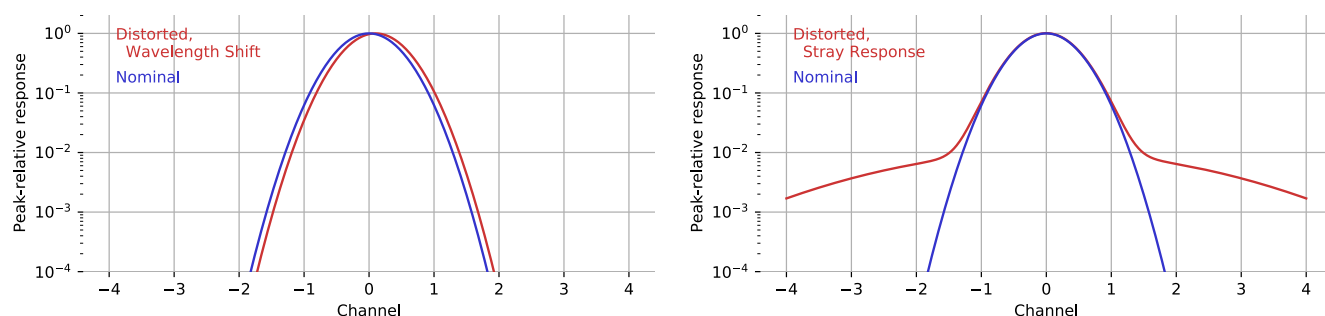


**Figure 3.** The spectral response function (SRF) under different spectroscopic distortions. Left: wavelength shift of 0.1 nm (10% of the channel spacing). Right: stray spectral response.

and structural composition (such as nitrogen content, chlorophyll, leaf mass, and lignin) using partial least squares regression, or PLSR (Wold et al., 2001). Once the model coefficients have been derived, this method is computationally efficient and has been applied to many remotely sensed data sets (Asner et al., 2015; Coops et al., 2003; Serbin et al., 2014; Singh et al., 2015; Townsend et al., 2003; Wang et al., 2019, 2020). It has shown good performance in a wide range of conditions, making it a primary candidate for SBG. However, PLSR requires significant initial training, and is sensitive to small systematic perturbations in the spectral input (Singh et al., 2015). Here we base our analysis on the models of Chadwick et al. (2020). That work was a regional study but typifies state of the art vegetation analysis that might apply on a broader scale to SBG. A training set of remote spectra and paired field measurements is used to train a PLSR model that predicts functional traits for tree canopy spectra. We select five moderately dense tree canopy spectra that represent the data set. We then apply the PLSR coefficients to estimate three canopy traits: leaf mass per area (LMA), which averaged  $399.2 \text{ g m}^{-2}$ ; nitrogen content (N), which averaged 2.25% of dry leaf mass; and leaf water content (LWC), which averaged 49.92% of fresh leaf mass. The original study used tenfold cross validation, resulting in ten models trained on different held out subpopulations. We take the average prediction of the models as the aggregate estimate.

The second benchmark case typifies a coastal aquatic study. Coastal and inland waters show diverse spectral shapes (Dekker et al., 2002) that reveal water column constituents such as phytoplankton pigments, carbon in particulate and dissolved forms, and suspended sediment (Hestir et al., 2015). These constituents can indicate water quality in inland water ecosystems and productivity in coastal regions. While many of these absorption signatures overlap, contemporary VSWIR imaging spectrometers provide sufficient spectral resolution to estimate them independently. Here we consider three well-understood water column constituents: chlorophyll, Colored Dissolved Organic Matter (CDOM), and sediments. We limit ourselves to the dominant phytoplankton pigment for simplicity, but more sophisticated community structure retrievals are possible (Cael et al., 2020; Kramer & Siegel, 2019) and will certainly be important for SBG. Water column constituent signals appear in the visible and UV wavelengths of water leaving reflectance spectra. Since these targets are dark, and the atmospheric scattering in short wavelengths is strong, the target signal is a small fraction of the measured radiance. Consequently, accurate atmospheric correction is critical. We

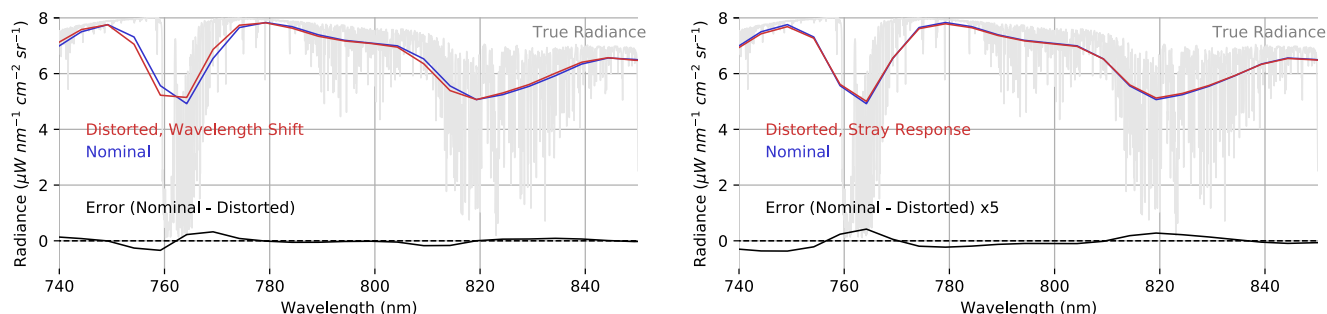


**Figure 4.** Effects of different distortions on measured radiance. The gray line refers to the actual radiance at sensor, shown with high spectral resolution. Left: Wavelength shift and associated residuals. Right: Stray spectral response and associated residuals.

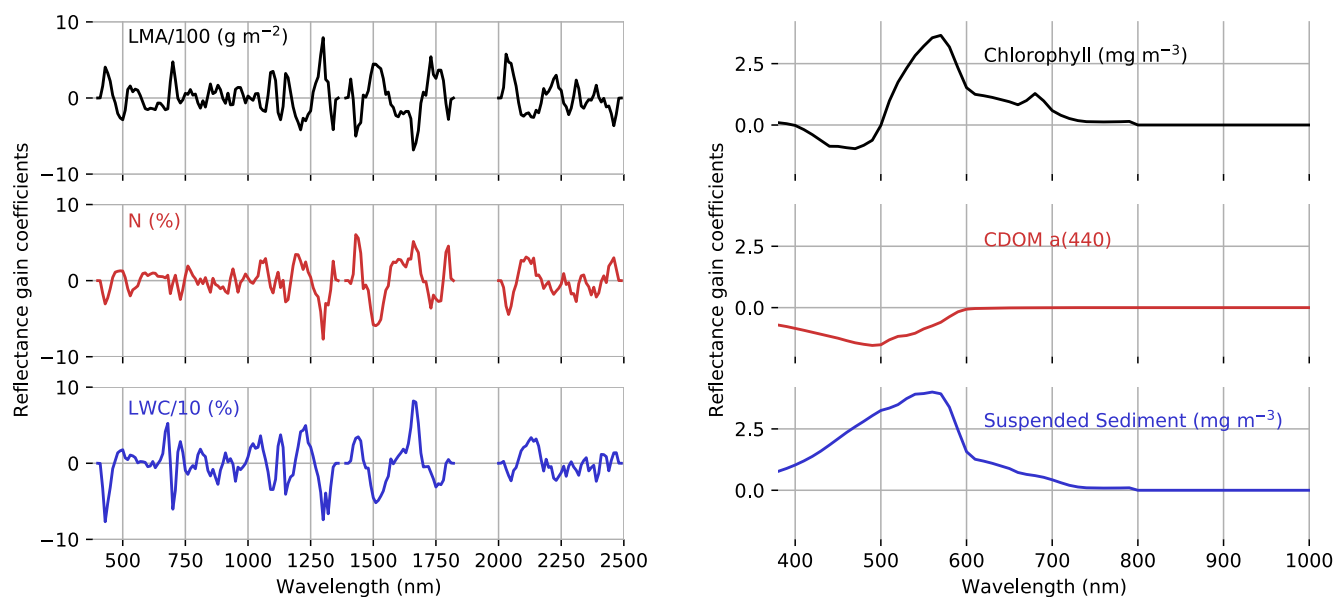


**Figure 5.** Gain coefficients for both terrestrial (Left) and aquatic (Right) inversion algorithms. They show the partial derivative of the estimate with respect to each reflectance channel. The partial least squares regression (PLSR) model at left oscillates rapidly, and is more sensitive to spectral nonuniformities than the smooth lookup table inversion at right.

use a water-leaving reflectance spectrum calculated using the Hydrolight RTM (Mobley, 1994), with assumptions typical of Case II coastal waters. We simulate ten spectra with chlorophyll *a* concentrations of 0.2–0.5  $\text{mg m}^{-3}$ , CDOM absorption of 0.1–0.3 at 440 nm, and sediment concentrations of 0.5–1  $\text{g m}^{-3}$ , all typical of continental shelf zones targeted by SBG. We calculate water-leaving reflectance at 1 nm spectral sampling and interpolate to SBG spectral sampling. Our inversion is a popular method similar to that of Mobley et al. (2005). In advance, we calculate a comprehensive table of water-leaving reflectance spectra for a wide range of parameter values. We then perform a least squares fit of the measured surface reflectance by adjusting the concentrations of chlorophyll, CDOM and suspended minerals, finding the associated model reflectance with multilinear interpolation in the lookup table.

Figure 5 shows the spectral gain coefficients (Rodgers, 2000) for both reflectance inversions. Gain coefficients represent the partial derivative of the estimate with respect to a change in the input reflectance for each channel. They are evaluated at the true state. These shapes indicate the reflectance changes which would increase the estimated quantity. For the PLSR model at left, the inversion is perfectly linear so the gain coefficients are the PLSR coefficients. For the aquatic case, the coefficients were calculated as in Rodgers (2000) using a local linearization of the lookup table reflectance model and uniform noise assumptions. The terrestrial coefficients show rapid oscillations and large first derivatives which make them sensitive to wavelength miscalibrations.

To transform terrestrial and aquatic reflectances into measured radiance we must posit a set of observing conditions. These observing conditions can influence sensitivity to wavelength miscalibration, since its impact depends on the depth and shape of gas absorption features. Rather than attempt to anticipate the distribution of SBG atmospheres, we simulate two different scenarios that span a range of conditions. Specifically, we consider observations of a surface at sea level with an atmosphere that is either dry or humid (with water vapor columns of 1.5 or 3  $\text{g cm}^{-2}$  respectively). We use haze free aerosol loading ( $\text{AOD} < 0.05$ ) in all cases. We evaluated performance for a solar zenith angle at 45°, a common situation in both tropical and midlatitude regions for a polar orbit with 10:30 h crossing time.

Following Vermote et al. (1997), our observation model relates the surface reflectance  $\rho_s$ , to the radiance at sensor  $\mathbf{L}_{obs}$  with the following expression:



$$\mathbf{L}_{obs} = \frac{\mathbf{E} \cos(\theta_s)}{\pi} \circ \left[ \rho_a + \frac{\mathbf{t}_{\downarrow} \mathbf{t}_{dir} \circ \rho_s}{1 - (\mathbf{s} \circ \rho_b)} + \frac{\mathbf{t}_{\downarrow} \mathbf{t}_{dif} \circ \rho_b}{1 - (\mathbf{s} \circ \rho_b)} \right] \quad (1)$$

Here,  $\theta_s$  is the solar zenith angle, and all other variables are vector-valued spectra with  $\circ$  representing element-wise multiplication.  $\mathbf{E}$  is the extrasolar irradiance,  $\rho_a$  is the path reflectance, and  $\mathbf{s}$  is the spherical sky albedo. The symbol  $\rho_b$  represents the reflectance of the background outside the pixel. The total downward transmittance along the sun to ground path is  $\mathbf{t}_{\downarrow}$ . The upward transmittance is written as a sum of a diffuse portion  $\mathbf{t}_{dif}$ , and a direct portion  $\mathbf{t}_{dir}$ . The total transmittance  $\mathbf{t}$  is the product of upward and downward transmittances. For an isotropic reflector following Lambert's cosine law, dividing by  $\pi$  converts the irradiance quantity  $\mathbf{E}$  into a radiance. We further simplify the model by taking the spatial reflectance field to be uniform, in which case  $\rho_s = \rho_b$ :

$$\mathbf{L}_{obs} = \frac{\mathbf{E} \cos(\theta_s)}{\pi} \circ \left[ \rho_a + \frac{\mathbf{t} \circ \rho_s}{1 - (\mathbf{s} \circ \rho_s)} \right] \quad (2)$$

We calculate values of  $\mathbf{s}$ ,  $\mathbf{t}$ , and  $\rho_a$  using the MODTRAN 6.0 RTM (Berk & Hawes, 2017) for a given atmospheric state. Our calculations use a high resolution  $0.1 \text{ cm}^{-1}$  correlated-k band model. Note that expression 2 assumes the surface is Lambertian. Accounting for photometric effects of observation geometry is outside the scope of this work; such treatments generally use empirical or geometric optical models that are insensitive to spectral calibration, so we can safely ignore them. After calculating the radiance at the sensor aperture, we add sensor noise to simulate the measurement process. We use instrument noise similar to the standard recommended by the Decadal Survey: a signal-to-noise ratio (SNR) of 400 in the Visible to Near infrared from 400 to 1,500 nm, and an SNR of 250 in the Shortwave Infrared from 1,500 to 2,500 nm. The Decadal Survey defined these SNR standards for a 25% reflective surface, so spatial averaging, or co-adding, might be necessary to achieve this noise level over dark aquatic targets. We apply random noise independently to every radiance channel, which is appropriate for photon shot noise, read noise, and electronic signal chain effects. We assume a channel spacing and spectral response full width at half maximum of 10 nm. We simulate measurements by resampling the high-resolution radiative transfer calculation using artificial wavelength offsets ranging from 0 to 2 nm in 0.2 nm increments, representing various degrees of spectral calibration shift. These offsets are applied uniformly to all channels, reflecting typical smile or shift-related errors in grating-based imaging spectrometers. Prism-based spectrometers might experience more severe transformations, such as wavelength-dependent changes in dispersion. We also apply a blurring operation representing off-nominal thick tails of the response function. Specifically, we construct a linear spectral blurring operator as in D. R. Thompson, Boardman et al. (2018). This thick tailed response is a second Gaussian line shape with a width that is, four times the main response, and a magnitude that varies from 0 to 0.0005 times that of the central peak. Naturally, different instruments may have many response function shapes, so our model provides only a rough indication of sensitivity to this parameter.

We invert the distorted radiance measurements using a Bayesian Maximum A Posteriori procedure similar to previous work (D. R. Thompson, Natraj, et al., 2018). This inversion aims to maximize the posterior probability of the state vector given the measurement, accounting for noise and prior background knowledge. We define a forward model  $\mathbf{F}(\mathbf{x})$  which transforms the state vector  $\mathbf{x}$  of surface and atmospheric parameters onto the radiance at the sensor  $\mathbf{L}_{obs}$ . The measurement  $\mathbf{y}$  is perturbed by random observation noise  $\epsilon$ :

$$\mathbf{y} = \mathbf{F}(\mathbf{x}) + \epsilon \quad (3)$$

The free parameters in the retrieval form a state vector  $\mathbf{x}$  containing the reflectance in every channel, and two additional values describing the aerosol optical depth and atmospheric water vapor concentration. The inversion estimates the most probable state given the measurement. In a Bayesian formalism this is equivalent to minimizing the cost function:

$$\chi(\mathbf{x}) = (\mathbf{F}(\mathbf{x}) - \mathbf{y})^T \mathbf{S}_\epsilon^{-1} (\mathbf{F}(\mathbf{x}) - \mathbf{y}) + (\mathbf{x} - \mathbf{x}_a)^T \mathbf{S}_a^{-1} (\mathbf{x} - \mathbf{x}_a) \quad (4)$$

The matrix  $\mathbf{S}_\epsilon$  represents the covariance of the zero mean observation noise. Its term penalizes departure of the modeled radiance from the measurement, weighted by the observation noise covariance. The second term of Equation 4 penalizes departure from the prior, a multivariate Gaussian with mean  $\mathbf{x}_a$  and covari-

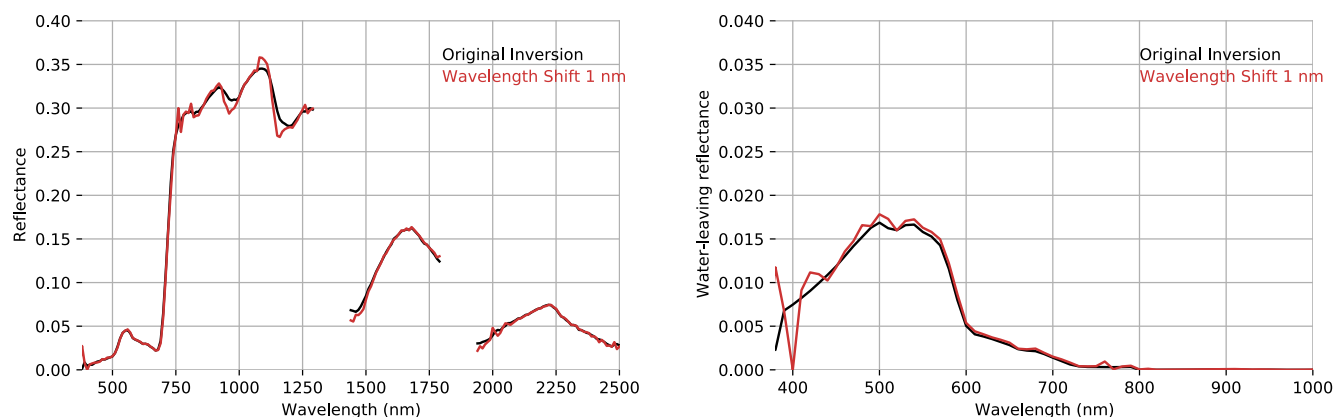


**Figure 6.** Vegetation and aquatic spectra used for this study, with characteristic errors that result from a 1 nm wavelength shift.

ance  $S_a$ . We construct a prior distribution following the procedure of D. R. Thompson et al. (2020), assuming atmospheric terms are independent. We form a surface prior using a wide range of terrestrial spectra from the USGS Spectral library (Kokaly et al., 2017), and a set of open water spectra described in D. R. Thompson, Cawse-Nicholson et al. (2019). As in D. R. Thompson et al. (2020), we use a conservative prior with all wavelengths uncorrelated outside the key water absorption windows. We also use regularization (Theiler, 2012) to ensure that the inversion can accurately reproduce shapes outside the envelope of library spectra. With this conservative uninformed prior, and haze-free scenes, the results are very similar to other alternative inversion methods based on differential optical absorption ratios (Schläpfer et al., 1998).

In order to evaluate the impact of the miscalibration-induced errors, we compare the magnitudes to: (a) the error induced by measurement noise alone; and (b) the background variability in ecosystems similar to what SBG would measure. For the second comparison, we use the standard deviation of traits from representative surveys in public literature. Terrestrial ecology traits use values taken from a multi-site study by Wang et al. (2020): the standard deviation of LMA is  $62.9 \text{ g m}^{-2}$ ; the standard deviation of N concentration is 0.72%, and the standard deviation of LWC is 7.9%. The standard deviation of marine ecosystem chlorophyll is  $0.275 \text{ mg m}^{-3}$ ; it comes from long-term observations of a Pacific Coastal ecosystem (Marrari et al., 2017). CDOM standard deviations of 0.11 (absorption at 440 nm) come from 36 months of observations in coastal waters by Keith et al. (2002). These only provide a rough indication of natural variability and may not represent all regions.

Figure 6 shows the reflectance spectra used for this study. The black line shows the inversion for a perfectly calibrated instrument. The red lines show the same result with a wavelength miscalibration of 1 nm. This is well within the range of shifts experienced by many historical instruments. The effect is most obvious in wavelengths with jagged, high contrast radiance structure. Artifacts appear in the near infrared region of the plant canopy from 750 to 1,300 nm, which includes a range of oxygen and water vapor features. The aquatic spectral range has less absorption by atmospheric gases, but shows artifacts in the shortest wavelengths near 400 nm that correspond to sharp solar absorption lines. We run 100 trials for each combination of distortions, atmospheres and spectra, and take the mean result.

### 3. Results

Figure 7 shows performance for the LMA model. The leftmost plot shows error as a function of spectral wavelength shift. The discrepancy at zero miscalibration is caused by instrument measurement error, but departures increase rapidly with larger miscalibrations. The black solid line is a polynomial fit to the data points for the dry atmospheric state, and the red solid line represents the humid atmospheric state. As expected, performance degrades more dramatically in humid conditions. The black dotted line represents the true value. A dark shaded area represents the variance due to retrieval noise, and a light gray shaded area represents the background variability (Wang et al., 2020). Error due to miscalibration exceeds the measurement noise at wavelength shifts of less than 0.25 nm, and it exceeds the background variability at wave-

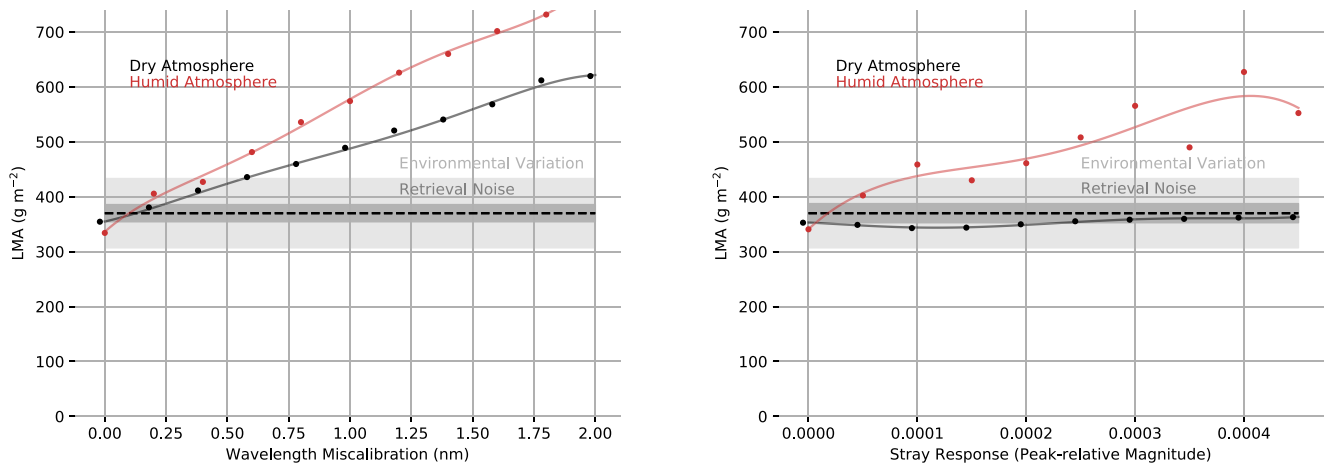


**Figure 7.** Errors induced by calibration errors for leaf mass per area (LMA) in dry and humid atmospheres. Shaded areas represent the uncertainty due to measurement noise in dark gray and the background variability in ecosystem traits from Wang et al. (2020) in light gray. The black dotted line shows the true value. Left: Errors due to spectral wavelength shift. Right: Errors due to stray spectral response.

length shifts between 0.35 and 0.6 nm. The rightmost plot shows the stray spectral response errors. These impacts depend even more strongly on ambient atmospheric conditions—the dry atmosphere is almost unaffected, while the humid atmosphere is strongly affected at stray response levels above 0.0001 times the peak response.

Figures 8 and 9 shows similar plots for the N and LWC traits. The impact of wavelength shifts, in the leftmost plots, are similar to LMA. As miscalibrations grow, these errors quickly exceed instrument noise. They eventually exceed background variability at shifts between 0.5 and 1.25 nm, with humid atmospheres always more sensitive than dry atmospheres. The effect of stray spectral response is also consistent; observations in dry atmospheres are nearly immune to spectral response error while observations in humid atmospheres are highly sensitive. N is severely impacted, exceeding background variability for even small amounts of spectral calibration error. These differences between dry and humid atmospheres would induce atmospheric biases in the trait retrieval, thwarting attempts to combine results across dry and humid atmospheres. These errors are particularly problematic because they masquerade as ecosystem-related signals in different vegetation, when in fact they are from the atmosphere. In general, the humidity-induced biases for

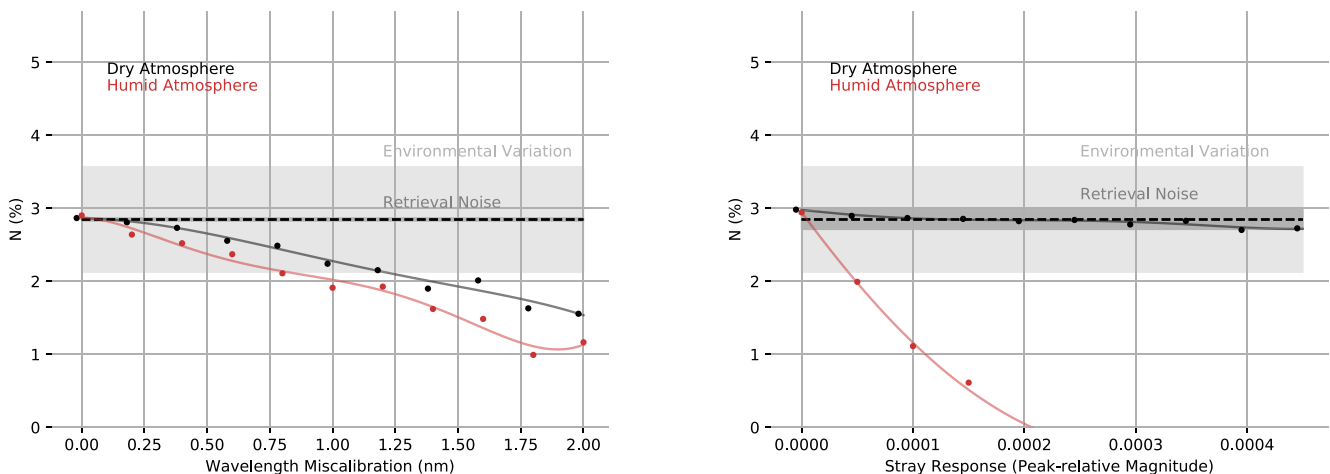


**Figure 8.** Errors in leaf nitrogen induced by calibration errors in dry and humid atmospheres. Shaded areas represent the uncertainty due to measurement noise and the background variability in ecosystem traits from Wang et al. (2020). The black dotted line shows the true value. Left: Errors due to spectral wavelength shift. Right: Errors due to stray spectral response.



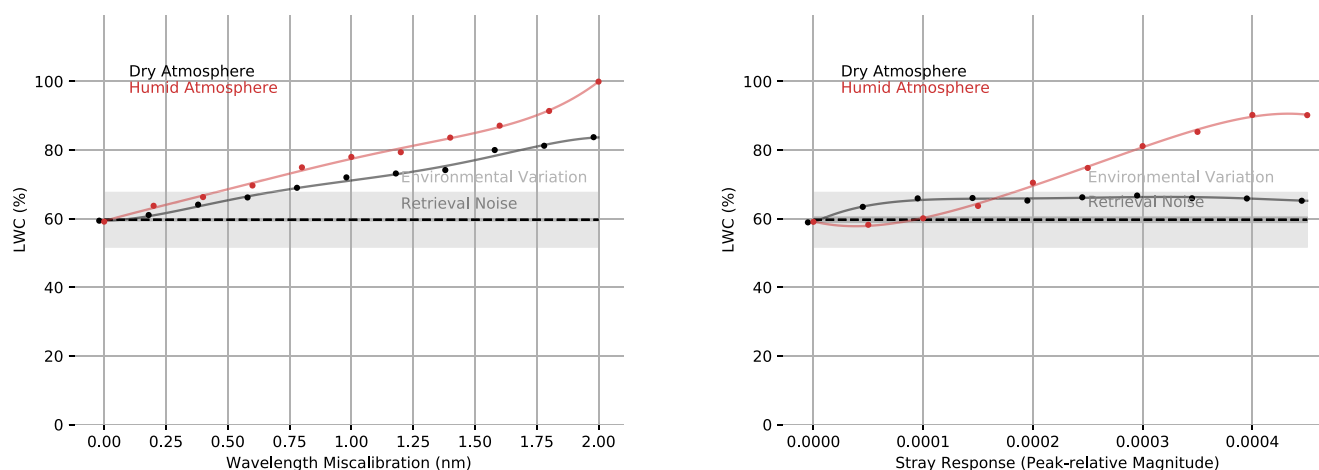


**Figure 9.** Errors induced by calibration errors for leaf water content (LWC) in dry and humid atmospheres. Shaded areas represent the uncertainty due to measurement noise and the background variability in ecosystem traits from Wang et al. (2020). The black dotted line shows the true value. Left: Errors due to spectral wavelength shift. Right: Errors due to stray spectral response.

these plant traits exceed the background variability at a spectral shift of 1.0 nm, and stray response magnitudes of less than 0.0001.

To quantify this effect we calculate shift-induced errors for different terrestrial biomes based on the annual mean water vapor content of their atmospheres. We correlate land cover maps from the University of Maryland land cover classification system (Defries & Hansen, 2010) and annualized MODIS mean water vapor estimates (Gao et al., 2015). This procedure indicates the mean water vapor content for each land cover class. Interpolating between our wet and dry errors yields a first-order approximation of the expected total error induced from spectral miscalibration for each land cover type. Table 1 shows the result for a wavelength offset of 1.0 nm. Clearly, high water vapor content in some biomes leads to more severe errors. This level of wavelength shift (which is nevertheless within historic bounds) induces the largest systematic errors in humid atmospheres, particularly the evergreen broadleaf forest cover type. Such systematic differences would complicate any attempt to apply a single model across multiple wide geographic areas.

**Table 1**

*Expected Systematic Errors in Percent for Each Vegetation Trait Induced by a 1 nm (10%) Wavelength Shift, as a Function of Atmospheres in Different Land Cover Type*

Land Cover Type	H <sub>2</sub> O(g cm <sup>2</sup> )	LMA Error(%)	N Error(%)	LWC Error(%)
Evergreen Needleleaf Forest	0.958	21	−18	36
Evergreen Broadleaf Forest	3.614	40	−39	76
Deciduous Needleleaf Forest	0.770	20	−16	33
Deciduous Broadleaf Forest	2.023	29	−26	52
Mixed Forest	1.213	23	−20	39
Woodlands	2.007	29	−26	51
Wooded Grasslands/Shrublands	1.101	22	−19	38
Closed Bushlands or Shrublands	1.869	28	−25	49
Open Shrubland	2.496	32	−30	59
Grasslands	1.119	22	−19	38
Croplands	1.647	26	−23	46

*Note.* Humid atmospheres, such as the broadleaf forests of tropical regions, are most heavily impacted. Predictions are based on the annual mean water vapor content for each land cover class.

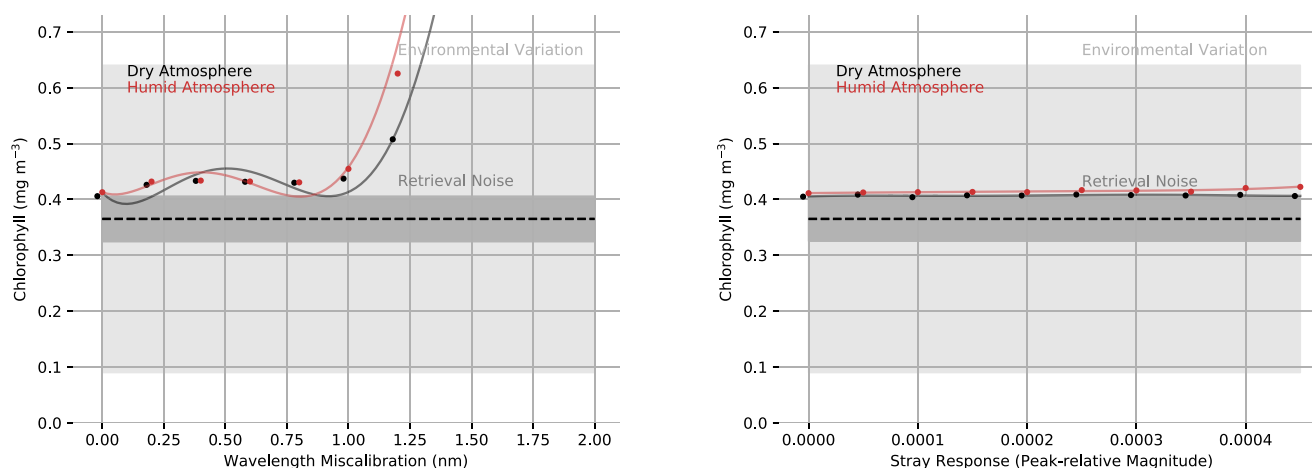


**Figure 10.** Errors induced by wavelength calibration errors for chlorophyll a estimation in dry and humid atmospheres. Shaded areas represent the uncertainty due to measurement noise and the background variability in ecosystem traits as described in the text. Left: Errors due to spectral wavelength shift Right: Errors due to stray spectral response.

As expected, the aquatic analyses are all less sensitive to spectral calibration error. Figures 10–12 show the result for chlorophyll, CDOM absorption at 440 nm, and suspended sediment, respectively. Again, the shaded areas represent measurement noise and background variability. As wavelength shift increases, performance initially degrades more gracefully than in the vegetation case, with errors of just 25% for a 1 nm shift. Wavelength shifts above 1.0 nm become increasingly detrimental, and even catastrophic for chlorophyll as residual artifacts grow around the sharp solar lines overlapping the 440 nm absorption feature. The other water column parameters show a similar degradation profile with very little effect until the 1.0 nm threshold is reached. Single-spectrum measurement errors due to noise alone are 5%–10% for all constituents. Neither dry nor humid atmospheres show any significant sensitivity to stray spectral response.

#### 4. Discussion

Our experiments demonstrate that the SBG investigation will be highly sensitive to spectral calibration error. In particular, SBG's terrestrial ecosystem objectives, as currently envisioned to use data driven trait models, will likely demand tighter calibration tolerances than previous missions such as Hyperion. The unique, global nature of the investigation, coupled with the subtle and spectrally dispersed nature of eco-

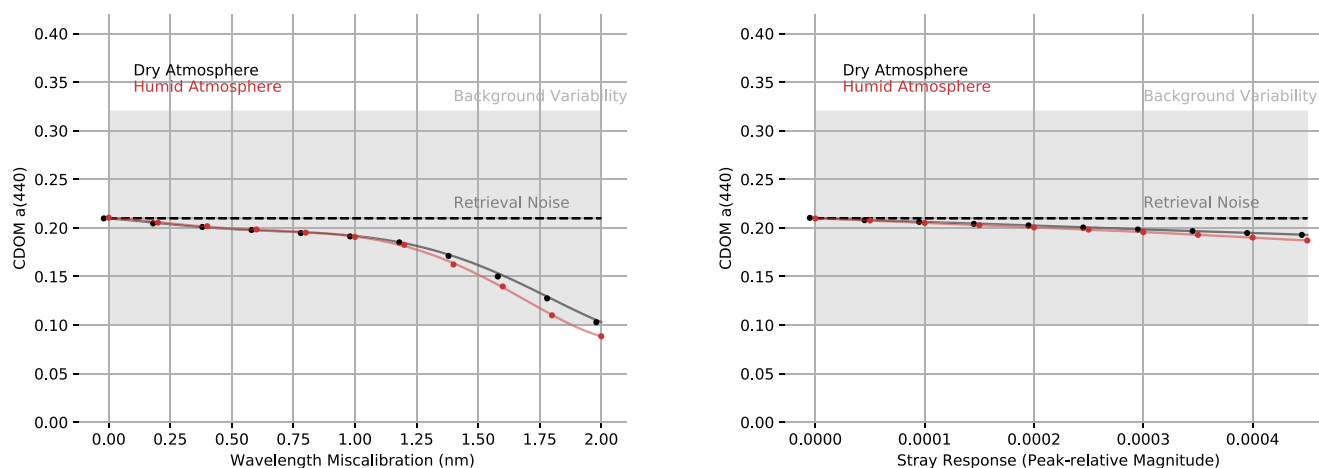


**Figure 11.** Errors induced by wavelength calibration errors for Colored Dissolved Organic Matter (CDOM) estimation in dry and humid atmospheres. Shaded areas represent the uncertainty due to measurement noise and the background variability in ecosystem traits as described in the text. The black dotted line shows the true value. Left: Errors due to spectral wavelength shift Right: Errors due to stray spectral response.

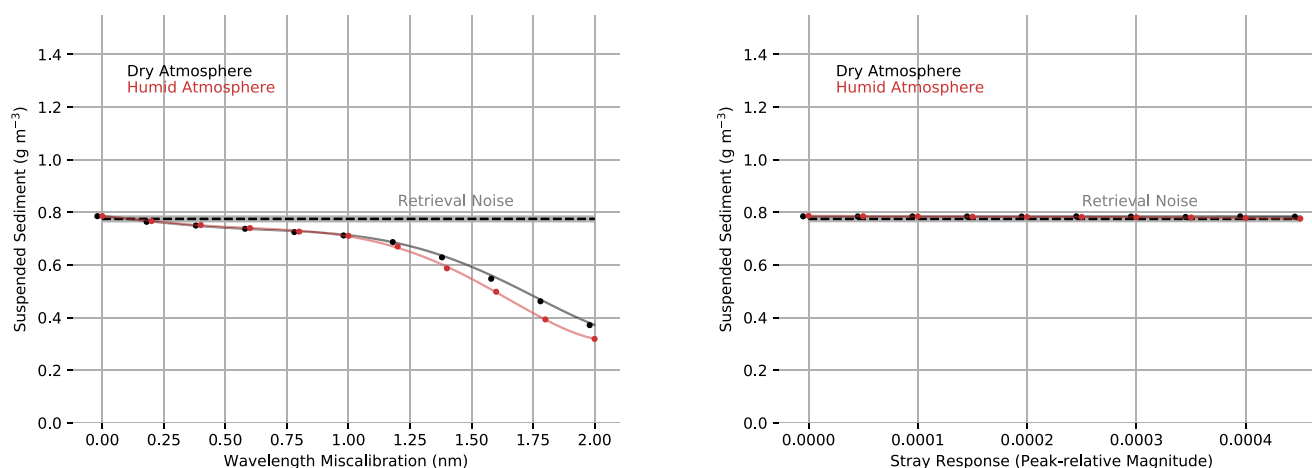


**Figure 12.** Errors induced by wavelength calibration errors for suspended sediment estimation in dry and humid atmospheres. A shaded area represents the uncertainty due to measurement noise. The black dotted line shows the true value. Left: Errors due to spectral wavelength shift Right: Errors due to stray spectral response.

system signals, means that small miscalibrations can have a significant impact on product accuracy and science yield. This extends upon earlier analysis by Green (1998), which demonstrated that wavelength shifts exceeding 1%–2% produce visible artifacts in reflectance spectra. Here we show that these artifacts affect the downstream biogeochemical measurements critical for SBG. Even inaccuracy of 5% (0.5 nm), a level which would traditionally have been considered safe for most applications, has a performance impact larger than the instrument noise. Higher levels become progressively more deleterious, inducing atmosphere-dependent biases that could impact comparisons across biomes or environmental gradients. More sophisticated aquatic retrievals, such as estimation of secondary pigments beyond chlorophyll *a* (Cael et al., 2020; Kramer & Siegel, 2019), could be similarly sensitive. Potential sources of these errors include wavelength drift over time, stray spectral response, and spatial non-uniformity of the wavelength calibration. All should be considered in the SBG design.

Historical missions show that adequate spectral calibration is achievable. Atmospheric features reveal the on-orbit spectral calibration from flight data (Guanter, Alonso, et al., 2006). These show that imaging spectrometers vary widely in wavelength calibration, spanning an order of magnitude in performance. The first orbital VSWIR imaging spectrometer, the Hyperion instrument onboard the EO-1 mission, achieved a cross-track spectral nonuniformity of 1.7–2.55 nm in the Visible Near InfraRed (VNIR) (Pearlman et al., 2001). At the other extreme, airborne instruments like the National Ecological Observation Network (NEON) Imaging Spectrometer have demonstrated uncorrected cross-track uniformity within 0.1 nm, or 2% of the channel spacing (Leisso et al., 2014). Between these extremes lie a range of calibration errors. Table 2 summarizes these wavelength shifts along with several performance thresholds in our study: the miscalibration levels equivalent to measurement noise, and those at which errors exceed the standard deviation of environmental variability. The result is sobering; to succeed, SBG must outperform most historical instruments.

There are several ways to prevent spectroscopy-induced trait errors. Combating drift is relatively easy, since atmospheric features provide an absolute standard to track wavelength calibration shifts over time. Future missions should operationalize this process to prevent avoidable errors. Wavelength inaccuracy caused by spatial nonuniformity is more challenging to address. One can resample the radiance data after acquisition, mapping different calibrations to a common wavelength grid. However, a 10 nm measurement grid generally undersamples the high-contrast atmospheric structure in radiance spectra. Consequently, resampling can cause errors such as distorted shapes or shifted band positions. Such corrections may not compensate completely for nonuniformities—for example, the DESIS mission software corrections reduced its spectral smile by approximately 38% (Alonso et al., 2019). An alternative might be to resample the reflectances instead, as in Goetz et al. (2003) or Richter et al. (2011). Specifically, one could run multiple radiative transfer calculations for different spectral calibrations, apply a specific model for atmospheric correction at each, and then resample the result in reflectance space where features are smoother and more amenable to

**Table 2**  
*Wavelength Calibration Error and Spatial Nonuniformity of Historical Instruments*

Wavelength Shift	Significance	References
0.1 nm	APEX <sup>a</sup>	Kuhlmann et al. (2016)
0.1 nm	NIS	Leisso et al. (2014)
0.1 nm	AVIRIS-NG	D. Thompson et al. (2015)
0.2 nm	Vegetation N error exceeds SBG measurement noise	This study
0.2 nm	CHRIS/PROBA	Guanter, Alonso, et al. (2006)
0.2 nm	CWIS	Corp et al. (2016)
0.4 nm	Vegetation N humidity bias exceeds SBG measurement noise	This study
0.5 nm	Vegetation LWC error exceeds environment variability	This study, Wang et al. (2020)
0.5 nm	ENMAP calibration requirement	Guanter et al. (2015)
0.55 nm	DESI <sup>a</sup>	Alonso et al. (2019)
1.0 nm	Vegetation LWC humidity bias exceeds environment variability	This study, Wang et al. (2020)
1.0 nm	Aquatic Chl error exceeds SBG measurement noise	This study
1.2 nm	HyMAP <sup>b</sup>	Guanter, Alonso, et al. (2006)
1.5 nm	Aquatic Chl error exceeds environment variability	This study, Marrari et al. (2017)
2.0 nm	ENMAP spectral smile requirement	Guanter et al. (2015)
2.0 nm	PRISMA spectral smile	Cogliati et al. (2021)
1.7–2.55 nm	Hyperion spectral smile	Pearlman et al. (2001)

*Note.* Rows indicate levels at which the shift-induced error exceeds other sources of variability in the measurement or environment. All comparisons use humid atmospheric conditions unless noted.

<sup>a</sup>A software correction was applied to achieve the reported performance. <sup>b</sup>Observed drift over one flight season.

interpolation. However, this approach is comparatively complex to implement. It still requires that the distortions be well characterized, and suffers some inevitable loss of information in sharp reflectance features or slopes. Finally, wavelength shifts are often a symptom of other miscalibration problems, such as field of view misregistration across channels. Resampling is a useful tool, but it is not a panacea.

Another remedy is to modify the retrieval methods to make them less susceptible to miscalibration errors. The terrestrial coefficients in our study are notable for having rapid oscillations and large first derivatives. This is common in empirical models of foliar traits, which often cue on very specific channel relationships (Wang et al., 2020). While the dominant compounds in tree canopies have broadband absorption features (Elvidge, 1990; Feret et al., 2008; Ustin et al., 2009), the expression of relevant biophysical differences is far subtler. This is at least partially due to the strong overlap between absorption coefficients (particularly in the SWIR), which requires algorithms to isolate specific spectral peaks from the otherwise smooth spectral regions. Importantly, although the sharp oscillatory structure in PLSR coefficients also appears in some other common trait estimation methods, it is not universal. On the contrary, trait retrieval methods that leverage physically based canopy RTMs (Berger et al., 2018; Verrelst et al., 2019) have broad and smooth spectral gain features that may be less susceptible to spectral precision and uniformity, to the point that some trait retrieval is even possible using multispectral sensors like Landsat (Houborg et al., 2015). However, compared to data-driven approaches, physically based approaches are typically more computationally intensive and are limited to a much smaller, though growing (Feret et al., 2008; Féret et al., 2017, 2021), set of target traits. Therefore, realizing the full potential of SBG for plant trait mapping depends on minimizing the spectral calibration issues raised in this manuscript.

Besides spectral resampling and better algorithms, perhaps the best and most elegant solution is simply to prioritize spectral calibration highly in instrument design. This should include consideration of both spatial uniformity and control of stray light. Adequate performance has been achieved by multiple historical

instruments, demonstrating that the desired level of performance is possible in practice without excessive cost. Designing to these standards will reap long-term dividends in algorithms that generalize better and translate more easily to partner instruments. In the design phase, modern tolerancing and error analyses (Moore et al., 2020) can provide rapid assessment of predicted optical performance and identification of driving tolerances, which can be used to improve uniformity and other key performance parameters. Modern alignment methods can validate the spectral response, spatial response, and uniformity characteristics prior to launch (Bender et al., 2011). For a global ecosystem study like SBG, no degree of wavelength shift should be considered “safe.” Spatial uniformity requirements should be established. Uniformity should be reported in descriptions of instrument performance alongside the more commonly quoted radiometric performance.

Stray spectral response is a slightly different problem. Its effects range from negligible under dry atmospheres, to extreme under more humid ones. This difference could induce ecosystem-dependent biases in global vegetation products. Unlike spectral calibration, which can be ensured by good optical design, alignment, and operational practices (Bender et al., 2011), stray spectral response depends on the scattering properties of different components that are more difficult to predict or change. Fortunately, stray response may also be more amenable to software corrections. Unlike the wavelength grid which under samples sharp reflectance shapes, the extended spectral response is oversampled by the focal plane array so the information exists to reconstruct the nominal measurement. Software approaches to characterizing and correcting spectral response functions have been demonstrated operationally for many years (D. R. Thompson, Boardman, et al., 2018; Kuhlmann et al., 2016; Zong et al., 2006). The extended spectral response function is measured in the laboratory or in flight, after which it can be deconvolved to restore a pristine Gaussian response. The upcoming EMIT mission (Green et al., 2020) may deploy this procedure operationally, offering a chance to evaluate whether such an approach will meet SBG needs.

Finally, we note some important caveats. This was intended as a sensitivity study based on a handful of representative but stressing example retrievals. It is concise rather than comprehensive, and the results of particular studies may not match these predicted impacts. It also ignores some other important errors that are more difficult to simulate, such as keystone distortions in which different wavelengths come from different locations on the surface. Finally, alternative retrieval algorithms or PLSR models might possibly achieve similar measurements with less sensitivity to spectral calibration error. Nevertheless, the fundamental conclusion—that terrestrial ecosystems require highly accurate spectral calibration—is consistent with previous work and should hold more generally.

## 5. Conclusions

This study investigates the impact of spectral calibration errors, in the form of wavelength calibration shifts and stray spectral response, on SBG objectives. We simulate these errors for inversion problems that are representative of aquatic and terrestrial ecology measurements. We show that inaccuracies which have been considered acceptable for previous missions can easily induce systematic error that is larger than the instrument noise and comparable to the variation in physical properties SBG aims to measure. Terrestrial ecosystem studies that rely on subtle delineations between spectral features of tree canopies are particularly sensitive to such errors. Previous orbital instruments have shown a wide range of spectral calibration accuracy. Surface measurements using PLSR favor the upper range of historical spectrometer performance to avoid errors exceeding not just the measurement noise, but even the background variability in terrestrial biomes. Investigators should be aware that even minor spectral miscalibration due to drift or spatial nonuniformity can induce systematic atmosphere-dependent errors in vegetation traits. Since vegetation community composition correlates strongly with these environmental factors, limiting such biases is important for building consistent global maps. Measuring and reducing stray spectral response should also be a primary concern. Despite these admonitions, the SBG investigation promises to revolutionize our understanding of terrestrial and aquatic ecosystems. All the performance targets implied by this study are achievable, or have been achieved, by historical instruments. Thus, with due attention to spectral calibration accuracy, there is reason for great optimism in the SBG endeavor.



## Data Availability Statement

Code used for the forward and inverse modeling can be found at the ISOFIT repository (<https://github.com/isofit/isofit>). Data used in the experiments can be found at zenodo, in a repository that is, available to reviewers and made fully public after acceptance for publication (<https://doi.org/10.5281/zenodo.3735479>).

## Acknowledgments

PAT was supported by a contract from JPL (award 1638464) and NASA (awards 80NSSC17K0677 and 80NSSC20K0208). SPS was supported by NASA contract #NNG20OB24A and by the United States Department of Energy contract No. DE-SC0012704 to Brookhaven National Laboratory. Contributions from ANS, BP and DRT were supported by the NASA Surface Biology and Geology (SBG) mission study. Contributions from KDC were supported by the National Science Foundation under Grant No. 1841547. This research was performed at the Jet Propulsion Laboratory, California Institute of Technology, under a contract with the National Aeronautics and Space Administration. Copyright 2021 California Institute of Technology. All rights reserved. US Government Support Acknowledged.

## References

- Alonso, K., Bachmann, M., Burch, K., Carmona, E., Cerra, D., de los Reyes, R., et al. (2019). Data products, quality and validation of the DLR earth sensing imaging spectrometer (DESI). *Sensors*, 19(20), 4471. <https://doi.org/10.3390/s19204471>
- Asner, G. P., Martin, R. E., Anderson, C. B., & Knapp, D. E. (2015). Quantifying forest canopy traits: Imaging spectroscopy versus field survey. *Remote Sensing of Environment*, 158, 15–27. <https://doi.org/10.1016/j.rse.2014.11.011>
- Bender, H. A., Mouroulis, P., Eastwood, M. L., Green, R. O., Geier, S., & Hochberg, E. B. (2011). Alignment and characterization of high uniformity imaging spectrometers. In *Imaging spectrometry xvi* (Vol. 8158, p. 81580J). <https://doi.org/10.1117/12.892798>
- Berger, K., Atzberger, C., Danner, M., D'Urso, G., Mauser, W., Vuolo, F., & Hank, T. (2018). Evaluation of the PROSAIL model capabilities for future hyperspectral model environments: A review study. *Remote Sensing*, 10(1). Retrieved from <https://www.mdpi.com/2072-4292/10/1/85>
- Berk, A., & Hawes, F. (2017). Validation of MODTRAN® 6 and its line-by-line algorithm. *Journal of Quantitative Spectroscopy and Radiative Transfer*, 203, 542–556. <https://doi.org/10.1016/j.jqsrt.2017.03.004>
- Cael, B., Chase, A., & Boss, E. (2020). Information content of absorption spectra and implications for ocean color inversion. *Applied Optics*, 59(13), 3971–3984. <https://doi.org/10.1364/ao.389189>
- Cavender-Bares, J., Gamon, J. A., & Townsend, P. A. (2020). Remote sensing of plant biodiversity. <https://doi.org/10.1007/978-3-030-33157-3>
- Cawse-Nicholson, K., Townsend, P. A., Schimel, D., Assiri, A. M., Blake, P. L., Buongiorno, M. F., et al. (2021). NASA's surface biology and geology designated observable: A perspective on surface imaging algorithms. *Remote Sensing of Environment*, 257, 112349. <https://doi.org/10.1016/j.rse.2021.112349>
- Ceamanos, X., & Douté, S. (2010). Spectral smile correction of CRISM/MRO hyperspectral images. *IEEE Transactions on Geoscience and Remote Sensing*, 48(11), 3951–3959. <https://doi.org/10.1109/tgrs.2010.2064326>
- Chadwick, K. D., Brodrick, P. G., Grant, K., Goulden, T., Henderson, A., Falco, N., et al. (2020). Integrating airborne remote sensing and field campaigns for ecology and Earth system science. *Methods in Ecology and Evolution*, 11(11), 1492–1508. <https://doi.org/10.1111/2041-210x.13463>
- Cogliati, S., Sarti, F., Chiarantini, L., Cosi, M., Lorusso, R., Lopinto, E., et al. (2021). The PRISMA imaging spectroscopy mission: Overview and first performance analysis. *Remote Sensing of Environment*, 262, 112499. <https://doi.org/10.1016/j.rse.2021.112499>
- Coops, N. C., Smith, M.-L., Martin, M. E., & Ollinger, S. V. (2003). Prediction of eucalypt foliage nitrogen content from satellite-derived hyperspectral data. *IEEE Transactions on Geoscience and Remote Sensing*, 41(6), 1338–1346. <https://doi.org/10.1109/tgrs.2003.813135>
- Dadon, A., Ben-Dor, E., & Karnieli, A. (2010). Use of derivative calculations and minimum noise fraction transform for detecting and correcting the spectral curvature effect (smile) in hyperion images. *IEEE Transactions on Geoscience and Remote Sensing*, 48(6), 2603–2612. <https://doi.org/10.1109/tgrs.2010.2040391>
- Defries, R., & Hansen, M. (2010). *ISLSCP II University of Maryland global land cover classifications, 1992–1993*. ORNL Distributed Active Archive Center. Retrieved from [http://daac.ornl.gov/cgi-bin/dsviewer.pl?ds\\_id=969](http://daac.ornl.gov/cgi-bin/dsviewer.pl?ds_id=969)
- Dekker, A. G., Brando, V. E., Anstee, J. M., Pinnel, N., Kutser, T., Hoogenboom, E. J., et al. (2002). Imaging spectrometry of water. In *Imaging spectrometry* (pp. 307–359). Springer. [https://doi.org/10.1007/978-0-306-47578-8\\_11](https://doi.org/10.1007/978-0-306-47578-8_11)
- DiVittorio, A. V. (2009). Enhancing a leaf radiative transfer model to estimate concentrations and in vivo specific absorption coefficients of total carotenoids and chlorophylls a and b from single-needle reflectance and transmittance. *Remote Sensing of Environment*, 113(9), 1948–1966. <https://doi.org/10.1016/j.rse.2009.05.002>
- Elvidge, C. D. (1990). Visible and near infrared reflectance characteristics of dry plant materials. *Remote Sensing*, 11(10), 1775–1795. <https://doi.org/10.1080/01431169008955129>
- Féret, J.-B., Berger, K., de Boissieu, F., & Malenovsky, Z. (2021). Prospect-pro for estimating content of nitrogen-containing leaf proteins and other carbon-based constituents. *Remote Sensing of Environment*, 252, 112173. <https://doi.org/10.1016/j.rse.2020.112173>
- Féret, J.-B., François, C., Asner, G. P., Gitelson, A. A., Martin, R. E., Bidel, L. P., et al. (2008). Prospect-4 and 5: Advances in the leaf optical properties model separating photosynthetic pigments. *Remote Sensing of Environment*, 112(6), 3030–3043. <https://doi.org/10.1016/j.rse.2008.02.012>
- Féret, J.-B., Gitelson, A., Noble, S., & Jacquemoud, S. (2017). Prospect-d: Towards modeling leaf optical properties through a complete lifecycle. *Remote Sensing of Environment*, 193, 204–215. <https://doi.org/10.1016/j.rse.2017.03.004>
- Gao, B.-C. (2015). *Modis atmosphere l2 water vapor product*. NASA MODIS Adaptive Processing System, Goddard Space Flight Center, USA. [https://doi.org/10.5067/MODIS/MOD05\\_L2.006](https://doi.org/10.5067/MODIS/MOD05_L2.006)
- Goetz, A. F., Kindel, B. C., Ferri, M., & Qu, Z. (2003). Hatch: Results from simulated radiances, aviris and hyperion. *IEEE Transactions on Geoscience and Remote Sensing*, 41(6), 1215–1222. <https://doi.org/10.1109/tgrs.2003.812905>
- Gorp, B. V., Mouroulis, P., Wilson, D. W., Green, R. O., Rodriguez, J. I., Liggett, E., & Thompson, D. R. (2016). Compact Wide Swath Imaging Spectrometer (CWIS): Alignment and laboratory calibration. In J. F. Silny & E. J. Ientilucci (Eds.), *Imaging spectrometry xxi* (Vol. 9976, pp. 10–17). SPIE. <https://doi.org/10.1117/12.2239080>
- Green, R. O. (1998). Spectral calibration requirement for Earth-looking imaging spectrometers in the solar-reflected spectrum. *Applied Optics*, 37(4), 683–690. <https://doi.org/10.1364/ao.37.000683>
- Green, R. O. (2001). Atmospheric water vapor sensitivity and compensation requirement for Earth-looking imaging spectrometers in the solar-reflected spectrum. *Journal of Geophysical Research: Atmospheres*, 106(D15), 17443–17452. <https://doi.org/10.1029/2000jd900799>
- Green, R. O., Mahowald, N., Ung, C., Thompson, D. R., Bator, L., Bennet, M., & Zan, J. (2020). *The Earth surface mineral dust source investigation: An Earth science imaging spectroscopy mission*. (pp. 1–15). IEEE.
- Guanter, L., Alonso, L., Gómez-Chova, L., & Moreno, J. (2006). Coupled approach for spectral/radiometric calibration and surface reflectance retrieval from CHRIS/PROBA data. In *Iv CHRIS/PROBA workshop*. ESA publications division.
- Guanter, L., Kaufmann, H., Segl, K., Foerster, S., Rogass, C., Chabrillat, S., et al. (2015). The EnMAP spaceborne imaging spectroscopy mission for Earth observation. *Remote Sensing*, 7(7), 8830–8857. <https://doi.org/10.3390/rs70708830>

- Guanter, L., Richter, R., & Moreno, J. (2006). Spectral calibration of hyperspectral imagery using atmospheric absorption features. *Applied Optics*, 45(10), 2360–2370. <https://doi.org/10.1364/ao.45.002360>
- Hestir, E. L., Brando, V. E., Bresciani, M., Giardino, C., Matta, E., Villa, P., & Dekker, A. G. (2015). Measuring freshwater aquatic ecosystems: The need for a hyperspectral global mapping satellite mission. *Remote Sensing of Environment*, 167, 181–195. <https://doi.org/10.1016/j.rse.2015.05.023>
- Houborg, R., McCabe, M., Cescatti, A., Gao, F., Schull, M., & Gitelson, A. (2015). Joint leaf chlorophyll content and leaf area index retrieval from Landsat data using a regularized model inversion system (REGFLEC). *Remote Sensing of Environment*, 159, 203–221. <https://doi.org/10.1016/j.rse.2014.12.008>
- Jetz, W., Cavender-Bares, J., Pavlick, R., Schimel, D., Davis, F. W., & Asner, G. P. (2016). Monitoring plant functional diversity from space. *Nature plants*, 2(3), 1–5. <https://doi.org/10.1038/nplants.2016.39>
- Keith, D., Yoder, J., & Freeman, S. (2002). Spatial and temporal distribution of coloured dissolved organic matter (CDOM) in Narragansett Bay, Rhode Island: Implications for phytoplankton in coastal waters. *Estuarine, Coastal and Shelf Science*, 55(5), 705–717. <https://doi.org/10.1006/ecss.2001.0922>
- Kokaly, R. F., Clark, R. N., Swayze, G. A., Livo, K. E., Hoefen, T. M., & Pearson, N. C. (2017). *USGS spectral library version 7* (Tech. Rep.). US Geological Survey.
- Kramer, S. J., & Siegel, D. A. (2019). How can phytoplankton pigments be best used to characterize surface ocean phytoplankton groups for ocean color remote sensing algorithms? *Journal of Geophysical Research: Oceans*, 124(11), 7557–7574. <https://doi.org/10.1029/2019jc015604>
- Kuhlmann, G., Hueni, A., Damm, A., & Brunner, D. (2016). An algorithm for in-flight spectral calibration of imaging spectrometers. *Remote Sensing*, 8(12), 1017. <https://doi.org/10.3390/rs8121017>
- Leisso, N., Kampe, T., & Karpowicz, B. (2014). Calibration of the national ecological observatory network's airborne imaging spectrometers. In *IEEE geoscience and remote sensing symposium* (pp. 2625–2628). <https://doi.org/10.1109/igarss.2014.6947012>
- Marrari, M., Piola, A. R., & Valla, D. (2017). Variability and 20-year trends in satellite-derived surface chlorophyll concentrations in large marine ecosystems around south and western Central America. *Frontiers in Marine Science*, 4, 372. <https://doi.org/10.3389/fmars.2017.00372>
- Mobley, C. D. (1994). *Light and water: Radiative transfer in natural waters*. Academic press.
- Mobley, C. D., Sundman, L. K., Davis, C. O., Bowles, J. H., Downes, T. V., Leathers, R. A., et al. (2005). Interpretation of hyperspectral remote-sensing imagery by spectrum matching and look-up tables. *Applied Optics*, 44(17), 3576–3592. <https://doi.org/10.1364/ao.44.003576>
- Moore, L. B., Bender, H. A., Bradley, C. L., Haag, J. M., Zandbergen, S., Green, R. O., & Mouroulis, P. (2020). Recent developments in tolerancing methods for imaging spectrometers. *Optical System Alignment, Tolerancing, and Verification, XIII*, 11488(114880B). <https://doi.org/10.1117/12.2568857>
- Mouroulis, P., Green, R. O., & Chrien, T. G. (2000). Design of pushbroom imaging spectrometers for optimum recovery of spectroscopic and spatial information. *Applied Optics*, 39(13), 2210–2220. <https://doi.org/10.1364/AO.39.002210>
- Myers, N., Mittermeier, R. A., Mittermeier, C. G., Da Fonseca, G. A., & Kent, J. (2000). Biodiversity hotspots for conservation priorities. *Nature*, 403(6772), 853–858. <https://doi.org/10.1038/35002501>
- National Academies of Sciences, Engineering, and Medicine. (2018). *Thriving on our changing planet: A decadal strategy for Earth observation from space*. National Academies Press. <https://doi.org/10.17226/24938>
- Neville, R. A., Sun, L., & Staenz, K. (2003). Detection of spectral line curvature in imaging spectrometer data, 5093, 144–154. <https://doi.org/10.4095/219993>
- Nieke, J., & Rast, M. (2018). Towards the copernicus hyperspectral imaging mission for the environment (chime). In *IGARSS 2018–2018 IEEE international geoscience and remote sensing symposium* (pp. 157–159). <https://doi.org/10.1109/igarss.2018.8518384>
- Nieke, J., Schlapfer, D., Dell'Endice, F., Brazile, J., & Itten, K. I. (2008). Uniformity of imaging spectrometry data products. *IEEE Transactions on Geoscience and Remote Sensing*, 46(10), 3326–3336. <https://doi.org/10.1109/tgrs.2008.918764>
- Pearlman, J., Carman, S., Segal, C., Jarecke, P., Clancy, P., & Browne, W. (2001). Overview of the Hyperion imaging spectrometer for the NASA EO-1 mission. In *IGARSS 2001. Scanning the present and resolving the future. Proceedings of IEEE 2001 international geoscience and remote sensing symposium*. (cat no 01ch37217). (Vol. 7), (pp. 3036–3038).
- Richter, R., Schl pfer, D., & M ller, A. (2010). Operational atmospheric correction for imaging spectrometers accounting for the smile effect. *IEEE Transactions on Geoscience and Remote Sensing*, 49(5), 1772–1780.
- Richter, R., Schl pfer, D., & M ller, A. (2011). Operational atmospheric correction for imaging spectrometers accounting for the smile effect. *IEEE Transactions on Geoscience and Remote Sensing*, 49(5), 1772–1780. <https://doi.org/10.1109/TGRS.2010.2089799>
- Rodgers, C. D. (2000). *Inverse methods for atmospheric sounding: Theory and practice* (Vol. 2). World scientific.
- Schimel, D., Townsend, P. A., & Pavlick, R. (2020). Prospects and pitfalls for spectroscopic remote sensing of biodiversity at the global scale. In *Remote sensing of plant biodiversity*. (pp. 503–518). Cham: Springer. [https://doi.org/10.1007/978-3-030-33157-3\\_19](https://doi.org/10.1007/978-3-030-33157-3_19)
- Schl pfer, D., Borel, C. C., Keller, J., & Itten, K. I. (1998). Atmospheric precorrected differential absorption technique to retrieve columnar water vapor. *Remote Sensing of Environment*, 65(3), 353–366. [https://doi.org/10.1016/s0034-4257\(98\)00044-3](https://doi.org/10.1016/s0034-4257(98)00044-3)
- Serbin, S. P., Singh, A., McNeil, B. E., Kingdon, C. C., & Townsend, P. A. (2014). Spectroscopic determination of leaf morphological and biochemical traits for northern temperate and boreal tree species. *Ecological Applications*, 24(7), 1651–1669. <https://doi.org/10.1890/13-2110.1>
- Shiklomanov, A. N., Dietze, M. C., Viskari, T., Townsend, P. A., & Serbin, S. P. (2016). Quantifying the influences of spectral resolution on uncertainty in leaf trait estimates through a Bayesian approach to RTM inversion. *Remote Sensing of Environment*, 183, 226–238. <https://doi.org/10.1016/j.rse.2016.05.023>
- Singh, A., Serbin, S. P., McNeil, B. E., Kingdon, C. C., & Townsend, P. A. (2015). Imaging spectroscopy algorithms for mapping canopy foliar chemical and morphological traits and their uncertainties. *Ecological Applications*, 25(8), 2180–2197. <https://doi.org/10.1890/14-2098.1>
- Swayze, G. A., Clark, R. N., Goetz, A. F., Chrien, T. G., & Gorelick, N. S. (2003). Effects of spectrometer band pass, sampling, and signal-to-noise ratio on spectral identification using the Tetracorder algorithm. *Journal of Geophysical Research: Planets*, 108(E9). <https://doi.org/10.1029/2002je001975>
- Theiler, J. (2012). The incredible shrinking covariance estimator. In *Automatic Target Recognition xxii* (Vol. 8391, p. 83910P). <https://doi.org/10.1117/12.918718>
- Thompson, D., Leifer, I., Bovensmann, H., Eastwood, M., Fladeland, M., Frankenberg, C., et al. (2015). Real-time remote detection and measurement for airborne imaging spectroscopy: A case study with methane. *Atmospheric Measurement Techniques*, 8(10), 4383–4397. <https://doi.org/10.5194/amt-8-4383-2015>

- Thompson, D. R., Babu, K., Braverman, A. J., Eastwood, M. L., Green, R. O., Hobbs, J. M., et al. (2019). Optimal estimation of spectral surface reflectance in challenging atmospheres. *Remote Sensing of Environment*, 232, 111258. <https://doi.org/10.1016/j.rse.2019.111258>
- Thompson, D. R., Boardman, J. W., Eastwood, M. L., Green, R. O., Haag, J. M., Mouroulis, P., & Van Gorp, B. (2018). Imaging spectrometer stray spectral response: In-flight characterization, correction, and validation. *Remote Sensing of Environment*, 204, 850–860. <https://doi.org/10.1016/j.rse.2017.09.015>
- Thompson, D. R., Braverman, A., Brodrick, P. G., Candela, A., Carmon, N., Clark, R. N., et al. (2020). Quantifying uncertainty for remote spectroscopy of surface composition. *Remote Sensing of Environment*, 247, 111898. <https://doi.org/10.1016/j.rse.2020.111898>
- Thompson, D. R., Cawse-Nicholson, K., Erickson, Z., Fichot, C. G., Frankenberg, C., Gao, B.-C., et al. (2019). A unified approach to estimate land and water reflectances with uncertainties for coastal imaging spectroscopy. *Remote Sensing of Environment*, 231, 111198. <https://doi.org/10.1016/j.rse.2019.05.017>
- Thompson, D. R., Natraj, V., Green, R. O., Helmlinger, M. C., Gao, B.-C., & Eastwood, M. L. (2018). Optimal estimation for imaging spectrometer atmospheric correction. *Remote Sensing of Environment*, 216, 355–373.
- Townsend, P. A., Foster, J. R., Chastain, R. A., & Currie, W. S. (2003). Application of imaging spectroscopy to mapping canopy nitrogen in the forests of the central Appalachian Mountains using Hyperion and Aviris. *IEEE Transactions on Geoscience and Remote Sensing*, 41(6), 1347–1354. <https://doi.org/10.1109/tgrs.2003.813205>
- Ustin, S. L., Gitelson, A. A., Jacquemoud, S., Schaepman, M., Asner, G. P., Gamon, J. A., & Zarco-Tejada, P. (2009). Retrieval of foliar information about plant pigment systems from high resolution spectroscopy. *Remote Sensing of Environment*, 113, S67–S77. <https://doi.org/10.1016/j.rse.2008.10.019>
- Vermote, E., El Saleous, N., Justice, C., Kaufman, Y., Privette, J., Remer, L., et al. (1997). Atmospheric correction of visible to middle-infrared EOS-MODIS data over land surfaces: Background, operational algorithm and validation. *Journal of Geophysical Research: Atmospheres*, 102(D14), 17131–17141. <https://doi.org/10.1029/97jd00201>
- Verrelst, J., Malenovsky, Z., Van der Tol, C., Camps-Valls, G., Gastellu-Etchegorry, J.-P., Lewis, P., et al. (2019). Quantifying vegetation biophysical variables from imaging spectroscopy data: A review on retrieval methods. *Surveys in Geophysics*, 40(3), 589–629. <https://doi.org/10.1007/s10712-018-9478-y>
- Wang, Z., Chlus, A., Geygan, R., Ye, Z., Zheng, T., Singh, A., & Townsend, P. A. (2020). Foliar functional traits from imaging spectroscopy across biomes in eastern North America. *New Phytologist*, 228, 494–511.
- Wang, Z., Townsend, P. A., Schweiger, A. K., Couture, J. J., Singh, A., Hobbie, S. E., & Cavender-Bares, J. (2019). Mapping foliar functional traits and their uncertainties across three years in a grassland experiment. *Remote Sensing of Environment*, 221, 405–416. <https://doi.org/10.1016/j.rse.2018.11.016>
- Wold, S., Sjöström, M., & Eriksson, L. (2001). PLS-regression: A basic tool of chemometrics. *Chemometrics and Intelligent Laboratory Systems*, 58(2), 109–130. [https://doi.org/10.1016/s0169-7439\(01\)00155-1](https://doi.org/10.1016/s0169-7439(01)00155-1)
- Zong, Y., Brown, S. W., Johnson, B. C., Lykke, K. R., & Ohno, Y. (2006). Simple spectral stray light correction method for array spectroradiometers. *Applied Optics*, 45(6), 1111–1119. <https://doi.org/10.1364/ao.45.001111>